SSNP133 - Cracking of a plate perforated with the cohesive models

Summary:

This test makes it possible to model the propagation ofux cracks in an elastic perforated plate.

Modeling A : Elements of joint, cohesive law CZM_LIN_REG
Modeling B : Elements with internal discontinuity, cohesive law CZM_EXP.
Modeling C : Elements of interface, cohesive law CZM_OUV_MIX
Modeling D : Elements of joint, cohesive law CZM_EXP_REG
Modeling E : Modeling XFEM, cohesive law CZM_EXP_REG. Grid conforms to the cracks.
Modeling F : Modeling XFEM, cohesive law CZM_EXP_REG. Grid triangles nonin conformity.
Modeling G : Modeling XFEM, cohesive law CZM_EXP_REG. Grid not structured.
Modeling H : Modeling XFEM, cohesive law CZM_LIN_REG. Grid conform to the cracks.
Modeling I : Modeling XFEM, cohesive law CZM_OUV_MIX. Grid conforms to the cracks.
Modeling J : Modeling XFEM, cohesive law CZM_OUV_MIX. Grid nonin conformity.

Local classification *ad hoc* cohesive elements (except $X-FEM$) is ensured by the order MODI_MAILLAGE and the keyword ORIE_FISSURE. The brutal opening of the cracks is ensured by the piloting of the loading available for each one of these laws (see [R7.02.11]).

1 Problem of reference

1.1 Geometry and loading

One considers a square plate on side $2000\,mm$ with a hole of ray $R=500\,mm$ centered in the direction vertical and decentred in the horizontal direction (see Figure 1.1-a). The plate admits a horizontal symmetry plane (AB') passing by the center of the hole. This symmetry can enable us to reduce our study to the higher half of the plate when that is possible.

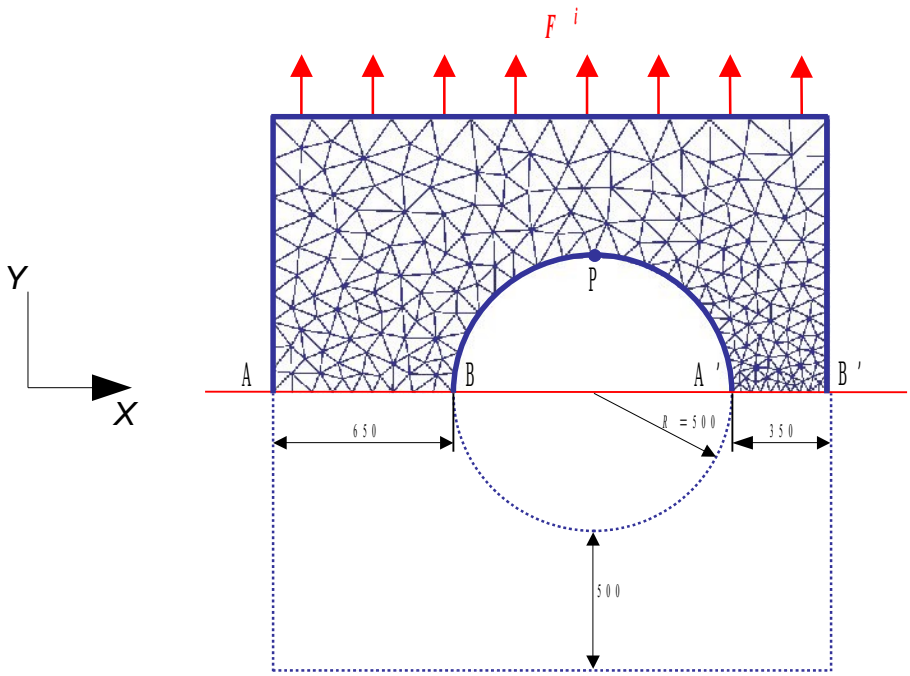

Figure 1.1-a : Diagram of the perforated plate, boundary conditions and loading.

One considers *a priori* that the cracks will develop along the axis of symmetry on both sides of the hole. One thus lays out the cohesive elements along the ways $[AB]$ and $[A'B']$. The loading consists in applying a density of surface force F^i unit directed in the direction Y on the upper part of the field. The intensity of this force will be given by the piloting of the loading (see [R7.02.11]). In addition, one imposes conditions of symmetry (worthless displacements according to Y) on the lower face of the cohesive elements. Lastly, one blocks the movements of rigid body by imposing a following null displacement X on the point P, top of the hole.

For modelings E with J, we have a formulation X-FEM: it is then necessary to model the whole structure for the moment. One introduces an interface on the line (AB'). One points out the approximation of the field of displacement for the nodes whose support is intersected by an interface XFEM:

$$\boldsymbol{u}_h(\boldsymbol{x})=\sum_i \Phi_i(\boldsymbol{x})\,\boldsymbol{a}_i+\sum_i \Phi_i(\boldsymbol{x})\,\boldsymbol{b}_i\,H\left(lsn(\boldsymbol{x})\right)$$

In order to block the movements of rigid body, it is wished that the interface be an axis of symmetry for the problem. If one considers M^+ and M^- points located immediately at the top and the lower part of the interface, we want that $u_y(M^+)+u_y(M^-)=0$.

For an interface in conformity, this implies $a_y=0$ on the nodes of the interface (figure 1.1-a).
For an interface not-in conformity which intersects the edges in their medium, while noting N_{SUP} and N_{INF} nodes in with respect to share and of other of the crack (figure 1.1-b), this implies:

$$a_y(N_{SUP})+a_y(N_{INF})=0$$

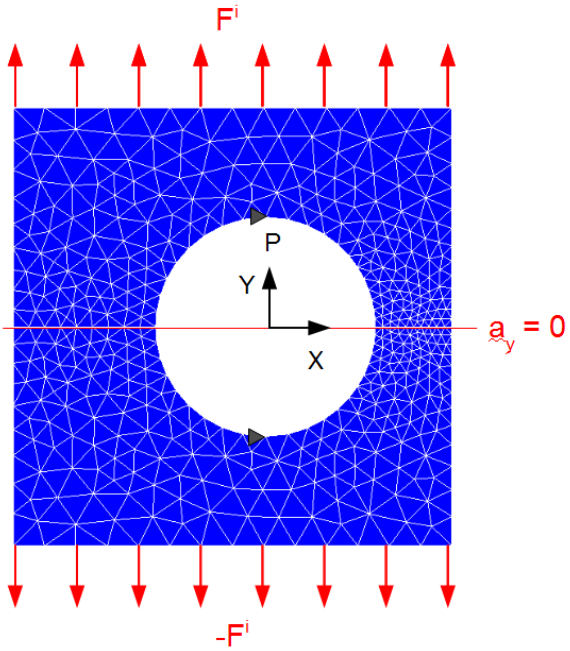

Figure 1.1-a: loading with a crack conforms.

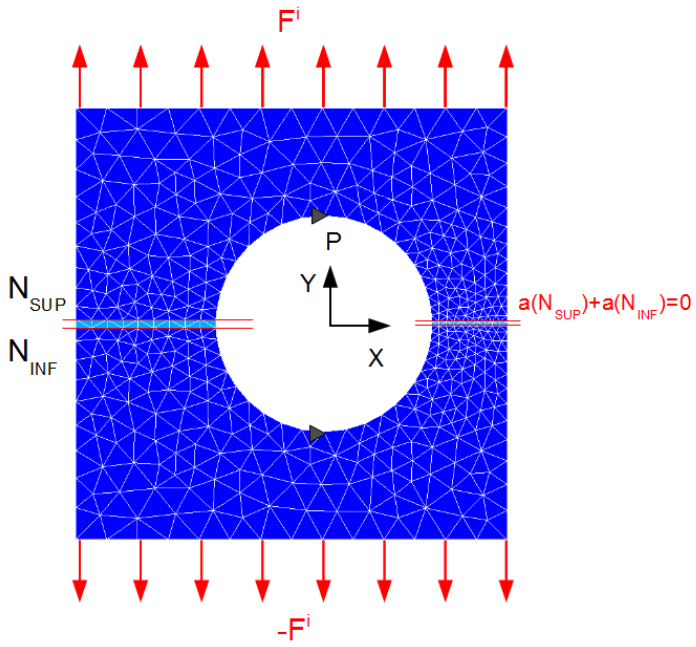

Figure 1.1-b: loading for a crack not-in conformity.

1.2 Properties material

The values of the Young modulus, of the Poisson's ratio, the critical stress and the tenacity of material are in the following way selected:

$$E=30000\,MPa \quad \nu=0.2 \quad \sigma_c=0.2\,MPa$$
$$G_c=100\,Pa.mm \quad \Rightarrow \quad \text{problème symétrisé}$$
$$G_c=200\,Pa.mm \quad \Rightarrow \quad \text{problème non symétrisé}$$

They are values “tests” which do not correspond to any material in particular. The purpose of the choice of the cohesive parameters is to obtain a solution with a relatively coarse grid. It is pointed out that to ensure a correct solution (precision and good convergence) with these models, it is necessary that there are several elements in the cohesive zone (see Doc. [U2.05.07]).

Note:

When the mechanical problem is symmetrized, one models only half of the cracks (only one lip).
These last dissipate an energy twice less important than if one had modelled the plate entirely.

To model a material of tenacity given G_c, it is thus necessary to carry out simulation with a value of $G_c / 2$.

2 Reference solution

There is no reference solution for this problem. Tests of nonregression are thus carried out. It is checked that the tests $XFEM$ the same results give as their counterparts FEM. For this reason, modeling D constitute a reference for modelings E with G, modeling A constitute a reference for modeling H and modeling C constitute a reference for modelings I and J.

3 Modeling A

3.1 Characteristics of modeling

The simulation of the propagation of the cracks by brittle fracture is carried out with modeling PLAN_JOINT and the law of behavior CZM_LIN_REG for the cohesive meshs. Voluminal elements, in plane deformations D_PLAN, are elastic.

3.2 Characteristics of the grid

One carries out a liné grid not structuredsurface of the perforated half-plate and the potential crack.
Voluminal elements (DCB): 404 TRIA3
Elements of joint (way of crack): 19 QUAD 4

3.3 Sizes tested and results

One carries out tests of nonregression on the total answer: F^i resultant of the force imposed on the higher face *versus* U displacement of the node P at the top of the hole.

Size tested	*Code_Aster*	*Tolerance (* $\%$ *)*
U at moment 50	3.3166D-03	0.10
F with moment 50	4.26153D+07	0.10
U with Instant 100	1.29488D-03	0.10
F withmoment 100	2.73873D+06	0.10
U with Instant 150	6.45752D-03	0.10
F withmoment 150	7.87206D+06	0.10
U with Instant 200	1.04754D-02	0.10
F withmoment 200	2.16189D+06	0.10

4 Modeling B

4.1 Characteristics of modeling

The simulation of the propagation of the cracks by brittle fracture is carried out with modeling PLAN_ELDI and the law of behavior CZM_EXP for the cohesive meshs. Voluminal elements, in plane deformations D_PLAN, are elastic.

4.2 Characteristics of the grid

One carries out a grid not structuré linear of the perforated half-plate and the potential crack.
Voluminal elements (DCB): 404 TRIA3
Elements with discontinuity interns (way of fissure) : 19 QUAD4

4.3 Sizes tested and results

One carries out tests of nonregression on the total answer: F^i resultant of the force imposed on the higher face *versus* U displacement of the node P at the top of the hole.

Size tested	*Code_Aster*	*Tolerance (* $\%$ *)*
U at moment 50	3.60651D-03	0.10
F withmoment 50	5.78832D+07	0.10
U with Instant 75	3.54604D-03	0.10
F withmoment 75	5.11117D+07	0.10
U with Instant 100	3.39435D-03	0.10
F withmoment 100	4.43684D+07	0.10
U with Instant 159	4.32977D-03	0.10
F withmoment 159	1.001265D+07	0.10

5 Modeling C

5.1 Characteristics of modeling

The simulation of the propagation of the cracks by brittle fracture is carried out with modeling PLAN_INTERFACE and the law of behavior CZM_OUV_MIX for the cohesive meshs. Voluminal elements, in plane deformations D_PLAN, are elastic.

5.2 Characteristics of the grid

One carries out a quadratic grid not structured of the perforated half-plate and potential crack.
Voluminal elements (DCB): 404 TRIA6
Elements of interface (way of crack): 19 QUAD8

5.3 Sizes tested and results

One carries out tests of nonregression on the total answer: F^i resultant of the force imposed on the higher face versus U displacement of the node P at the top of the hole.

Size tested	*Code_Aster*	*Tolerance (%)*
U at moment 50	2.87853E-03	0.10
F withmoment 50	2.88263E+07	0.10
U with Instant 75	6.55609E-03	0.10
F withmoment 75	1.04922E+07	0.10
U with Instant 100	7.47879E-03	0.10
F withmoment 100	4.94452E+06	0.10
U with Instant 140	0.0157679	0.10
F withmoment 140	8.56080E+05	0.10

6 Modeling D

6.1 Characteristics of modeling D

The simulation of the propagation of the cracks by brittle fracture is carried out with modeling PLAN_JOINT and the law of behavior CZM_EXP_REG for the cohesive meshs. Voluminal elements, in plane deformations D_PLAN, are elastic.

6.2 Characteristics of the grid

One carries out a linear grid not structured of the perforated half-plate and potential crack.
Voluminal elements (DCB): 804 TRIA3
Elements of joint (way of crack): 19 QUAD4

6.3 Sizes tested and results

One carries out tests of nonregression on the total answer: F^i resultant of the force imposed on the higher face versus U displacement of the node P at the top of the hole.

Size tested	Code_Aster	Tolerance (%)
U at moment 50	3.32215D-03	0.10
F withmoment 50	4.21054D+07	0.10
U with Instant 100	2.52359D-03	0.10
F withmoment 100	5.3546D+06	0.10
U with Instant 150	7.09118D-03	0.10
F withmoment 150	6.75039D+06	0.10

It is seen that the penalization of the cohesive law introduces a light difference between the results. If we thus compare the results of modeling D with those of B, we have the curved force-displacement of the figure 6.3-a.

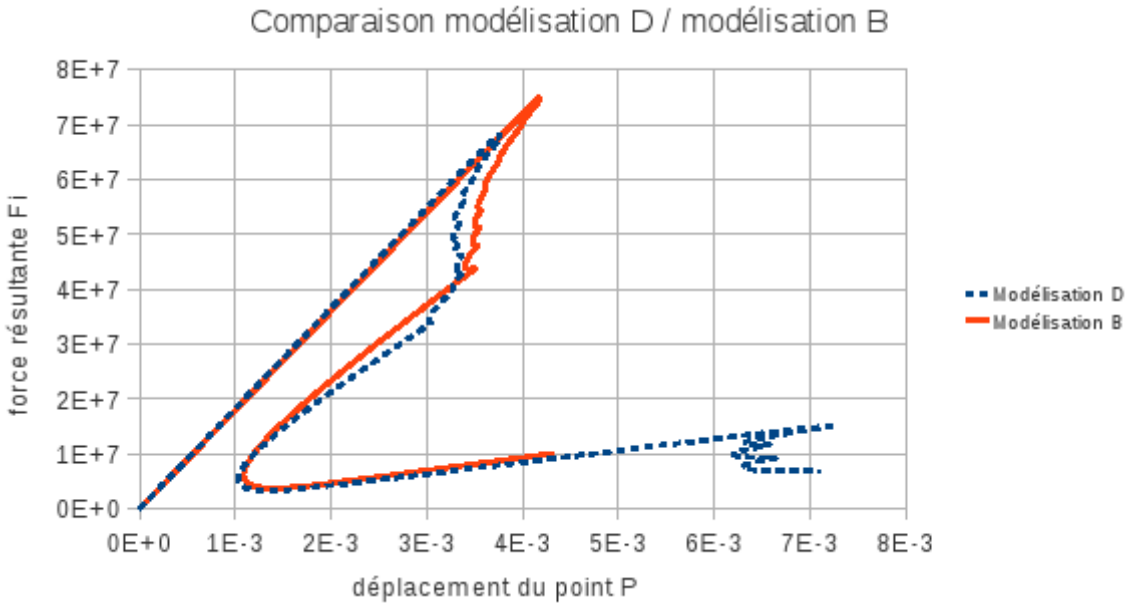

Figure 6.3-a: comparison elements of joint with elements with internal discontinuity.

7 Modeling E

7.1 Characteristics of modeling E

An interface of equation $[Y=0]$ is introduced into the model using a formulation XFEM, via a level set normal. The simulation of the propagation of the cracks by brittle fracture is carried out thanks to a relation of the type CZM_EXP_REG between constraint and jump of displacement enters the lips of the interface. Syntactically, this relation is included in the definition of a zone of contact between the two lips of the crack, with integration FPG3 or FPG2 and in formulation CZM. This means that the contact is managed by the cohesive law and that there is no friction. Physically, we find ourselves then rigorously in the same situation as modeling D. Voluminal elements, in plane deformations D_PLAN, are elastic.

7.2 Characteristics of the grid

One carries out a grid of the plate perforated in conformity with the crack.
Voluminal elements (DCB): 804 TRI3

7.3 Sizes tested and results

Modeling D is used as reference. One sees on the figure 7.3-a that the results are perfectly superposable.

Size tested	Type of Reference	Code_Aster	Tolerance (%)
U at moment 50	AUTRE_ASTER	3.32215D-03	0.10
F withmoment 50	AUTRE_ASTER	4.21054D+07	0.10
U with Instant 100	AUTRE_ASTER	2.52359D-03	0.10
F withmoment 100	AUTRE_ASTER	5.3546D+06	0.10
U with Instant 150	AUTRE_ASTER	7.09118D-03	0.10
F withmoment 150	AUTRE_ASTER	6.75039D+06	0.10

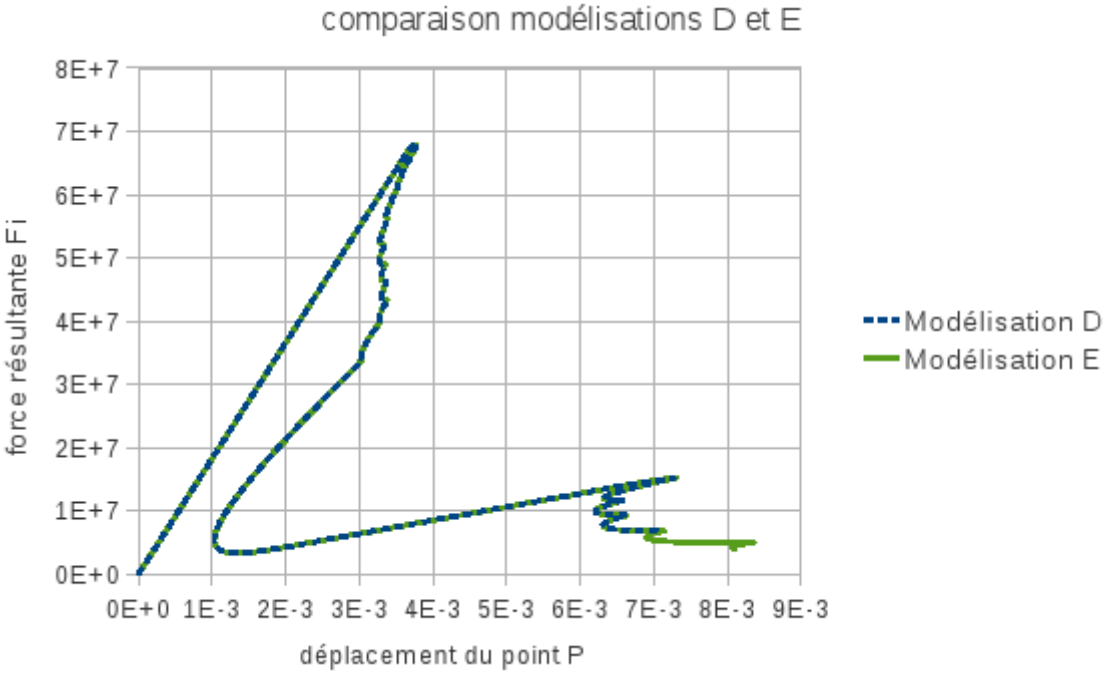

Figure 7.3-a: adequacy of modeling D with modeling E

7.4 Comments

Solutions FEM are superposable with the solutions $XFEM$ who have the same cohesive law. Consequently, this test makes it possible to validate the implementation $XFEM$ cohesive law, like that of piloting by elastic prediction.

8 Modeling F

8.1 Characteristics of modeling F

The characteristics of modeling are strictly identical to modeling E. Only the grid differs.

8.2 Characteristics of the grid

One carries out a grid of the plate entirely triangular, not-in conformity with the crack, such as certain intersected edges are nonvital.
Voluminal elements (DCB): 842 `TRI3`

8.3 Sizes tested and results

The beginning of calculation requires a little more subdivisions than modeling E. Taking into account this difference in the sequences in subdivision, the results of modelings E and F slightly different are compared urgent per moment. On the other hand, one sees on the figure 8.3-a that they are superposable. Having proven this correspondence, one thus takes for value of reference of nonregression those of modeling F.

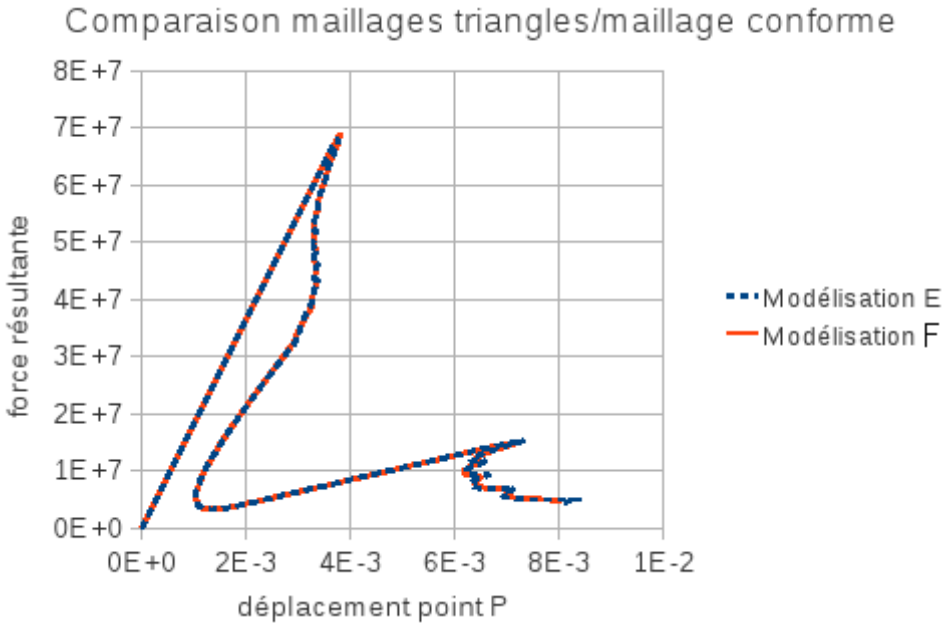

Figure 8.3-a: Comparison grid triangles/grid conforms

Size tested	Type of reference	Code_Aster	Tolerance (%)
U at moment 50	NON_REGRESSION	3.34481D-03	0.10
F withmoment 50	NON_REGRESSION	4.26501D+07	0.10
U with Instant 100	NON_REGRESSION	2.28519D-03	0.10
F withmoment 100	NON_REGRESSION	4.85041D+06	0.10
U with Instant 150	NON_REGRESSION	6.83775D-03	0.10
F withmoment 150	NON_REGRESSION	6.86061D+06	0.10

9 Modeling G

9.1 Characteristics of modeling G

The characteristics of modeling are strictly identical to modeling E. Only the grid differs.

9.2 Characteristics of the grid

One carries out a grid of the entirely triangular plate, not regulated. Certain edges are in conformity with the crack. Some are intersected.
Voluminal elements (DCB): 698 TRI3

9.3 Results of modeling G

One gets a result slightly different from modeling D. This is unlike grid between two modelings. Small the snap-backs is of origin digital and related to the refinement of the grid. They are larger here because the grid is less refined (fig.9.3-a). One thus changes the values of reference for the same reasons as modeling F.

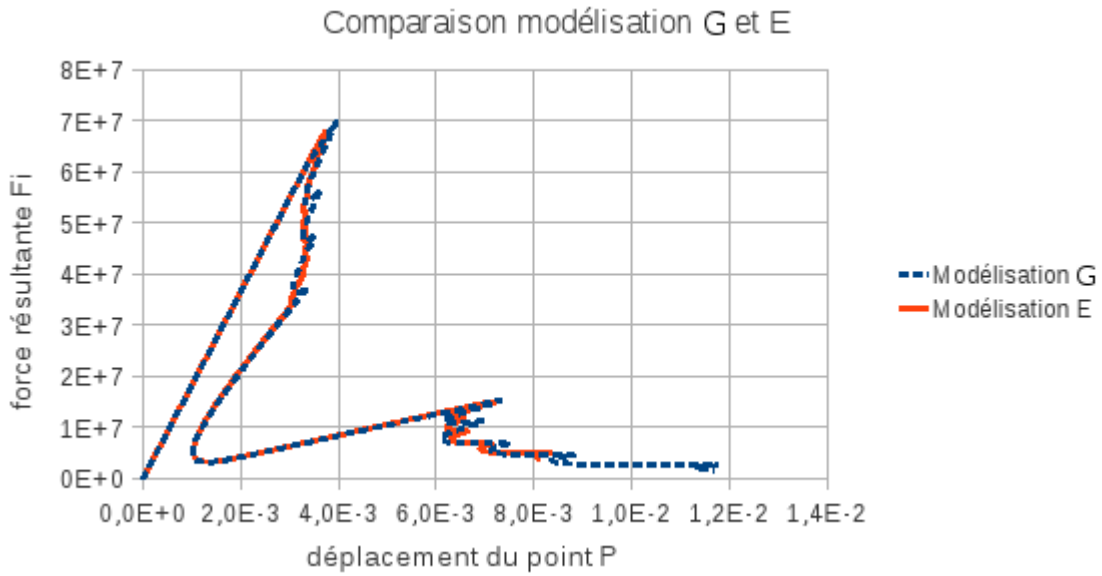

Figure 9.3-a: comparison between modelings G and E

Size tested	*Type of reference*	*Code_Aster*	*Tolerance (%)*
U at moment 50	NON_REGRESSION	3.21777D-03	0.10
F withmoment 50	NON_REGRESSION	3.6512D+07	0.10
U with Instant 100	NON_REGRESSION	7.41292D-03	0.10
F withmoment 100	NON_REGRESSION	1.54984D+07	0.10
U with Instant 150	NON_REGRESSION	7.76637D-03	0.10
F withmoment 150	NON_REGRESSION	4.65793D+06	0.10

10 Modeling H

10.1 Characteristics of modeling H

L be characteristic of modeling are strictly identical to those of modeling E . Only the cohesive law differs: the law CZM_LIN_REG is used.

10.2 Characteristics of the grid

The grid is the same one as that of modeling E . Let us recall that it is in conformity with the crack. Voluminal elements (DCB): 804 SORTING3.

10.3 Results of modeling H

Modeling A is used as reference. The results are perfectly superposable.

Size tested	Type of reference	Code_Aster	Tolerance ($\%$)
U at moment 50	AUTRE_ASTER	3.3166D-03	0.10
F withmoment 50	AUTRE_ASTER	4.26153D+07	0.10
U with Instant 100	AUTRE_ASTER	1.29488D-03	0.10
F withmoment 100	AUTRE_ASTER	2.73873D+06	0.10
U with Instant 150	AUTRE_ASTER	6.45752D-03	0.10
F withmoment 150	AUTRE_ASTER	7.87206D+06	0.10

11 Modeling I

11.1 Characteristics of modeling I

Characteristics of modeling E are taken again, except for the cohesive law. One uses the mixed law CZM_OUV_MIX. Consequently, grid of modeling E is made quadratic, and one defines in the operator MODI_MODELE_XFEM a discretization P2P1 for the contact.

11.2 Characteristics of the grid

The grid is the same one as that of modeling E. Let us recall that it is in conformity with the crack.
Voluminal elements : 804 SORTING 6.

11.3 Results of modeling I

Modeling C is used as reference. The layouts of the answers for two modelings are perfectly superposable.

Size tested	*Code_Aster*	*Tolerance (%)*
U at moment 50	2.8872E-03	0.10
F withmoment 50	2.8603E+07	0.10
U with Instant 75	6.43269E-03	0.10
F withmoment 75	9.8916E+06	0.10
U with Instant 100	7.8109E-03	0.10
F withmoment 100	4.7092E+06	0.10
U with Instant 140	2.2116E-02	0.10
F withmoment 140	6.24908E+05	0.10

12 Modeling J

12.1 Characteristics of modeling J

The characteristics of modeling are strictly identical to modeling I. Only the grid differs.

12.2 Characteristics of the grid

One carries out a grid of the entirely triangular plate, not regulated. Certain edges are in conformity with the crack. Some are intersected.
Voluminal elements (DCB): 698 SORTING6.

12.3 Results of modeling J

One gets a result slightly different from modeling I. This is unlike grid between two modelings. Small the snap-backs is of origin digital and related to the refinement of the grid. They are larger here because the grid is refined less. One thus changes the values of reference.

Size tested	*Type of reference*	*Code_Aster*	*Tolerance ($\%$)*
U at moment 50	NON_REGRESSION	2.9189E-03	0.10
F withmoment 50	NON_REGRESSION	2.9439E+07	0.10
U with Instant 75	NON_REGRESSION	6.6043E-03	0.10
F withmoment 75	NON_REGRESSION	1.0854E+07	0.10
U with Instant 100	NON_REGRESSION	7.2936E-03	0.10
F withmoment 100	NON_REGRESSION	5.2103E+06	0.10
U with Instant 140	NON_REGRESSION	0.014454	0.10
F withmoment 140	NON_REGRESSION	9.5855E+05	0.10

13 Summary of the results

The cohesive models make it possible qualitatively to simulate the brutal propagation of two cracks in brittle fracture through a perforated plate. The total answers of the seven models (in terms of force-displacement) are appreciably the same ones. The piloting of the loading makes it possible to follow the brutal rupture of the two ligaments on both sides of hole, leading to two “back return” in the total answer.